IPP-Report

Max-Planck-Institut
für Plasmaphysik

E. Strumberger and E. Schwarz

VACFIELD CODE:
COMPUTATION OF THE VACUUM MAGNETIC FIELD AND ITS FIRST DERIVATIVES FOR VARIOUS COIL TYPES

IPP 5/112
May 2005

TABLE OF CONTENTS

ABSTRACT

The VACFIELD code is used to compute the magnetic field of external coils. It determines the vacuum field and its first derivatives in cylindrical co-ordinates on a two- or three-dimensional grid. The conductors are approximated by straight pieces of infinitely thin current filaments. Various coil types of tokamak and stellarator devices are implemented. It is possible to choose between two different data formats of the magnetic field output. One serves as input to the MFBE and GOURDON codes, while the other one is used by the VMEC/NEMEC code.

1. INTRODUCTION

The vacuum magnetic field produced by external coils is the basis of a plasma equilibrium. While in stellarators toroidal and poloidal field components are mainly produced by external coil currents, in tokamaks a toroidal plasma current generates most of the poloidal field. There, poloidal field coils cause only a weak poloidal field, which is used for plasma shaping and controlling. In general, stellarator and tokamak fields have a three-dimensional geometry, but for many applications the small toroidal field ripple of tokamak fields is neglected. That is, the toroidal field of tokamaks is mostly approximated by the axisymmetric field of a straight and infinitely long conductor.

The VACFIELD code computes the magnetic field of external coils using Biot-Savart's law. The magnetic field and its first derivatives are determined on a two- or three-dimensional grid for various coil types of stellarator and tokamak devices. The following coil types are implemented in the code:

a.) main field coils: toroidal field coils and modular coils,

b.) correction coils: poloidal field coils and saddle coils,

c.) additional coils: helical coils and auxiliary coils.

The conductors are represented by straight pieces of closed, infinitely thin filaments.

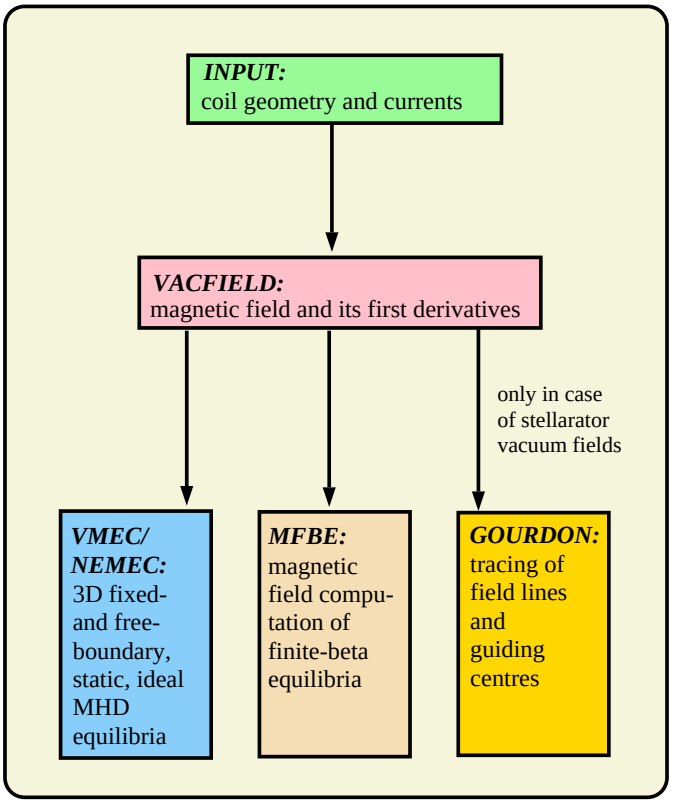

Fig. 1: Overview of the code system

The computed vacuum magnetic field serves as input to several codes as illustrated in Fig. 1. These codes are the free-boundary VMEC/NEMEC equilibrium code [1, 2], the magnetic field solver for finite-β equilibria (MFBE) code [3, 4], and the GOURDON code, which traces field lines and guiding centres. It is possible to choose between two different data formats of the magnetic field output. One serves as input to the MFBE and GOURDON codes, while the other one is used by the VMEC/NEMEC code.

Details of the VACFIELD code, numerical methods, and implemented coil types are described in the following sections. In Sect. 2 the geometries of various coil types are discussed. The definition of the grid, and the computation of the magnetic field and its first derivatives on that grid are the subjects of section 3. Details of the code, that is, the code structure (Sect. 4.1), input files (Sect. 4.2) and ouput files (Sect. 4.3) are described in Sect. 4. Accuracy tests are presented in section 5. Finally, in Appendix A coil sets available for ASDEX Upgrade (AUG), Wendelstein 7-X (W7-X) [5] and possible Helias stellarator reactors (HSR) [6] are listed. In Appendix B mathematical details are given concerning the computation of the first derivatives of the magnetic field, the transformation of the field components from Cartesian into cylindrical co-ordinates, and the use of the stellarator symmetry.

2. VARIOUS COIL TYPES

Three kinds of coils are distinguished with respect to their use:

1.) Main field coils producing the main magnetic field.

2.) Correction coils used for:

a.) plasma shaping and controlling of the plasma position,

b.) correction of field errors, and

c.) sweeping the strike points of the outflowing plasma on the divertor plates.

3.) Additional coils used for:

a.) creation of additional helical fields in tokamaks, and

b.) variation of the rotational transform and shift of the magnetic axis in stellarators.

2.1 MAIN FIELD COILS

Various types of main field coils are described in the following. First, the axisymmetric approximation of the torodial tokamak field is discussed. Second, the torodial field coils of the ASDEX Upgrade tokamak are described. And, finally, the modular coils of the W7-X stellarator are presented.

2.1.1 AXISYMMETRIC APPROXIMATION

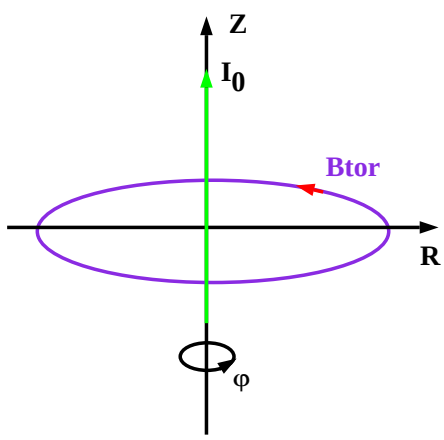

Fig. 2: A current, $\mathbf{I}_0$, along the Z-axis produces an axisymmetric, toroidal magnetic field, $\mathbf{B}_{\text{tor}}$, in φ-direction.

In tokamaks the main field produced by external coils is a purely toroidal field. The finite number of toroidal field coils destroys the perfect axisymmetry of the device. The coils produce

a short wavelength ripple in the magnetic field strength. Neglecting this field ripple, the toroidal field is usually approximated by an axisymmetric field. A straight and infinitely long conductor along the Z-axis would produce such an axiymmetric field in φ-direction (see Fig. 2). The corresponding magnetic field strength, B_{tor}, decreases in radial direction.

$$B_{\text{tor}} = \frac{\mu_0}{2\pi}\frac{I_0}{R} \tag{1}$$

2.1.2 TOROIDAL FIELD COILS

While the axisymmetric field approximation described above is mostly sufficient for equilibrium and stability studies of tokamaks, the toroidal magnetic field ripple ($\approx 1\%$ of the magnetic field strength) plays an important role with respect to the confinement of trapped particles.

ASDEX Upgrade toroidal field coils

ASDEX Upgrade has 16 planar, D-shaped toroidal field coils. In Fig. 3 the approximation of a coil by a single current filament is shown, while in Fig. 4 its geometrical representation is explained.

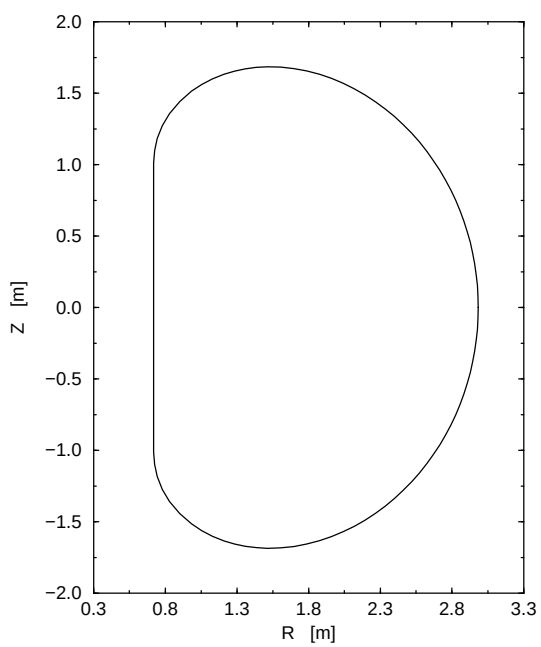

Fig. 3: Current filament.

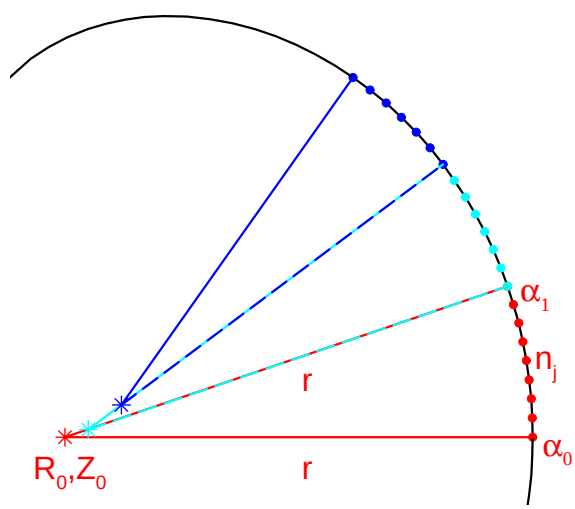

Fig. 4: Geometrical representation.

The D-shaped current filament is composed of N circular segments with centres (R_0^i, Z_0^i) and radii, r_i. Their poloidal boundaries are given by α_0^i and α_1^i $(i = 1, \ldots, N)$. As illustrated in Fig. 4,

every segment is approximated by M^i straight conductor pieces, n^i_j ($j = 1, \ldots, M^i$). The explicit data for the upper half of the current filament are given in Sect. 4.2.2.

A three-dimensional representation of the toroidal field coils is shown in Fig. 6 (Sect. 2.2.1).

2.1.3 MODULAR COILS

In stellarators, such as the helical advanced W7-X stellarator [5], the main field is produced by three-dimensional, complex-shaped modular coils. Because of the complex coil shape, the main field has toroidal and poloidal components which form already closed, nested magnetic surfaces.

W7-X modular coils

The five-periodic W7-X stellarator has 50 modular coils with 10 coils per period. Because of the stellarator symmetry and the five periods, the 50 modular coils consist of five different coil types only. In Fig. 5 the modular coils are shown for three periods.

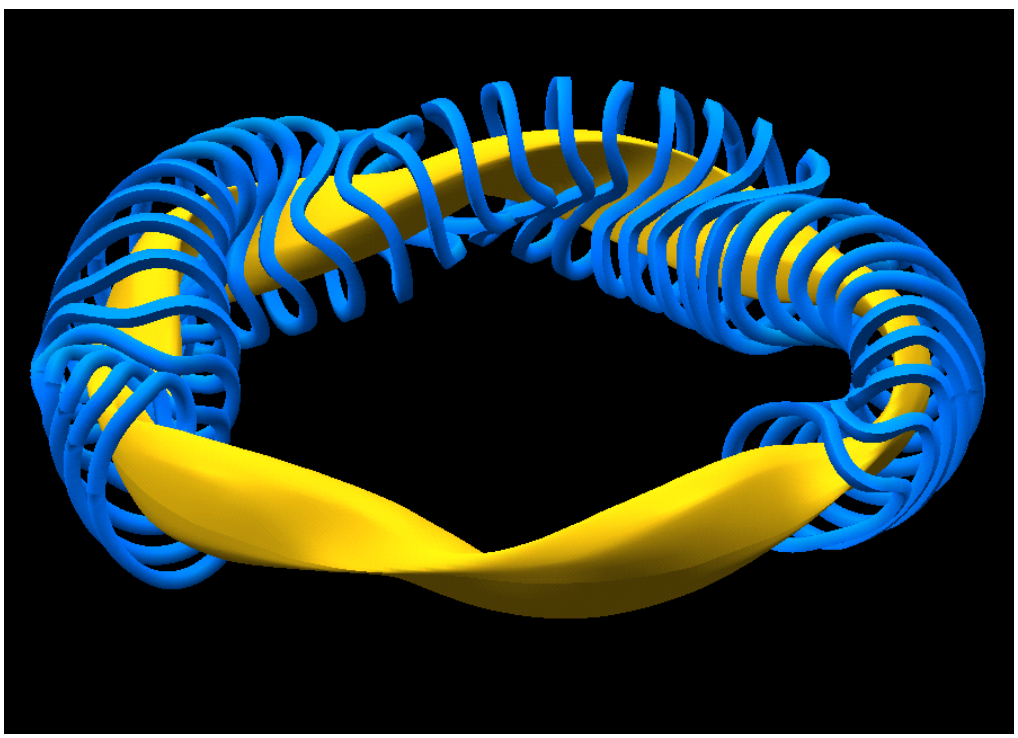

Fig. 5: Plasma surface (yellow) and modular coils (blue) of W7-X for three periods.

For the vacuum field computations, the coils are approximated by poloidally closed, infinitely thin filaments represented by a finite number of straight pieces (for more details see Sect. 4.2.2).

2.2 CORRECTION COILS

In tokamaks correction coils produce a week poloidal field which is used for plasma shaping and controlling of the plasma position. In stellarators corrections coils are used for the correction of small error fields, and for sweeping the strike points of the outflowing plasma on the divertor target plates in order to prevent excessive heat load on these plates.

2.2.1 POLOIDAL FIELD COILS

In tokamaks a set of axisymmetric poloidal field coils is used as correction coils.

ASDEX Upgrade poloidal field coils

ASDEX Upgrade has 13 active poloidal field coils (OH1, OH2o, OH2u, ...) and two passive conductors (pslon and pslun) for plasma shaping and controlling. These coils are shown in Fig. 6.

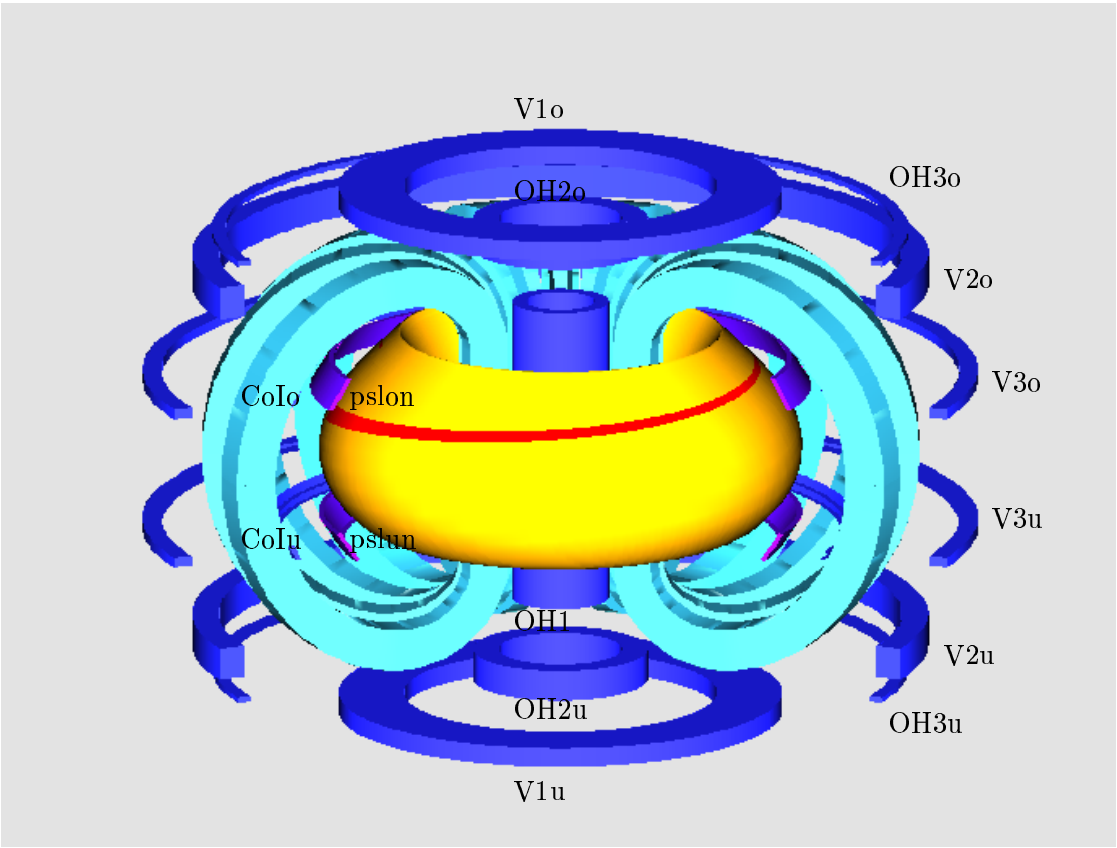

Fig. 6 Passive conductors (violet), and poloidal (blue) and toroidal (cyan) field coils of ASDEX Upgrade with plasma surface (yellow).

The poloidal field coils are centred around the symmetry axis of ASDEX Upgrade. Because of their elongated shapes in radial (e.g. OH2o and OH2u) and/or Z-direction (e.g. OH1), every coil i is represented by M_i infinitely thin, circular current filaments with currents I_i^j, radii, R_i^j, Z-co-ordinates, Z_i^j, and numbers of windings per filament, m_i^j ($j = 1, \ldots, M_i$). In the VACFIELD code each circular current filaments is approximated by L straight conductor pieces. The input of these coil data is described in detail in Sect. 4.2.3.

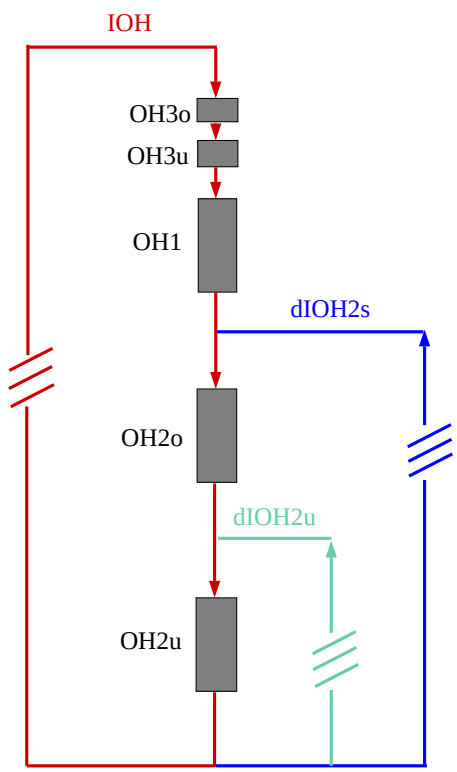

Fig. 7: Circuit diagram of the OH coils.

The coils OH1, OH2o, OH2u, OH3o and OH3u are connected in the circuit shown in Fig. 7. The following currents are defined:

$$I_{\mathrm{OH}} = \mathrm{IOH} \cdot (N_{\mathrm{OH1}} + N_{\mathrm{OH2o}} + N_{\mathrm{OH2u}} + N_{\mathrm{OH3o}} + N_{\mathrm{OH3u}}) \tag{2}$$

$$I_{\mathrm{OH2od}} = \mathrm{dIOH2s} \cdot N_{\mathrm{OH2o}} \tag{3}$$

$$I_{\mathrm{OH2ud}} = \mathrm{dIOH2s} \cdot N_{\mathrm{OH2o}} + \mathrm{dIOH2u} \cdot N_{\mathrm{OH2u}} \tag{4}$$

$$I_{\mathrm{OH1}} = \mathrm{IOH} \cdot N_{\mathrm{OH1}} \tag{5}$$

$$I_{\mathrm{OH2o}} = (\mathrm{IOH} + \mathrm{dIOH2s}) \cdot N_{\mathrm{OH2o}} \tag{6}$$

$$I_{\mathrm{OH2u}} = (\mathrm{IOH} + \mathrm{dIOH2s} + \mathrm{dIOH2u}) \cdot N_{\mathrm{OH2u}} \tag{7}$$

$$I_{\mathrm{OH3}} = \mathrm{IOH} \cdot (N_{\mathrm{OH3o}} + N_{\mathrm{OH3u}}) \tag{8}$$

$$I_{\mathrm{OH13}} = \mathrm{IOH} \cdot (N_{\mathrm{OH1}} + N_{\mathrm{OH3o}} + N_{\mathrm{OH3u}}) \tag{9}$$

The total number of windings of coil i, N_i (e.g. N_{OH1}), is given by the sum of windings per coil filament

$$N_i = \sum_{j=1}^{M_i} m_i^j. \tag{10}$$

2.2.2 SADDLE COILS

The implementation of so-called *saddle* or *sweep* coils is planned in W7-X [7] close to the divertor plates. For example, these coils will be used for the compensation of symmetry breaking error fields. By means of a periodically variating coil current, the coils will produce an oscillating magnetic field which will sweep the particle and head load areas across the divertor plates. For this reason, the coils are also called sweep coils. They, further, will control the variation of the connection length and modify the distance between target plates and separatrix.

Figure 8 shows one of ten saddle coils. For the numerical calculations these coils are represented in the same way as the modular coils of W7-X (for details see Sect. 4.2.2).

Fig. 8: Technical representation of a saddle coil (J. Kißlinger)

2.3 ADDITIONAL COILS

To improve experimental flexibility and physical properties, additional coils are implemented in some tokamak and stellarator devices.

2.3.1 HELICAL COILS

In the DIII-D tokamak, for example, additional coils have been implemented in order to damp neoclassical tearing modes by producing a week helical field [8]. In Fig. 9 six helical coils are plotted schematically together with the plasma surface, which is coloured due to the helical magnetic field strength (for details see Sect. 4.2.4).

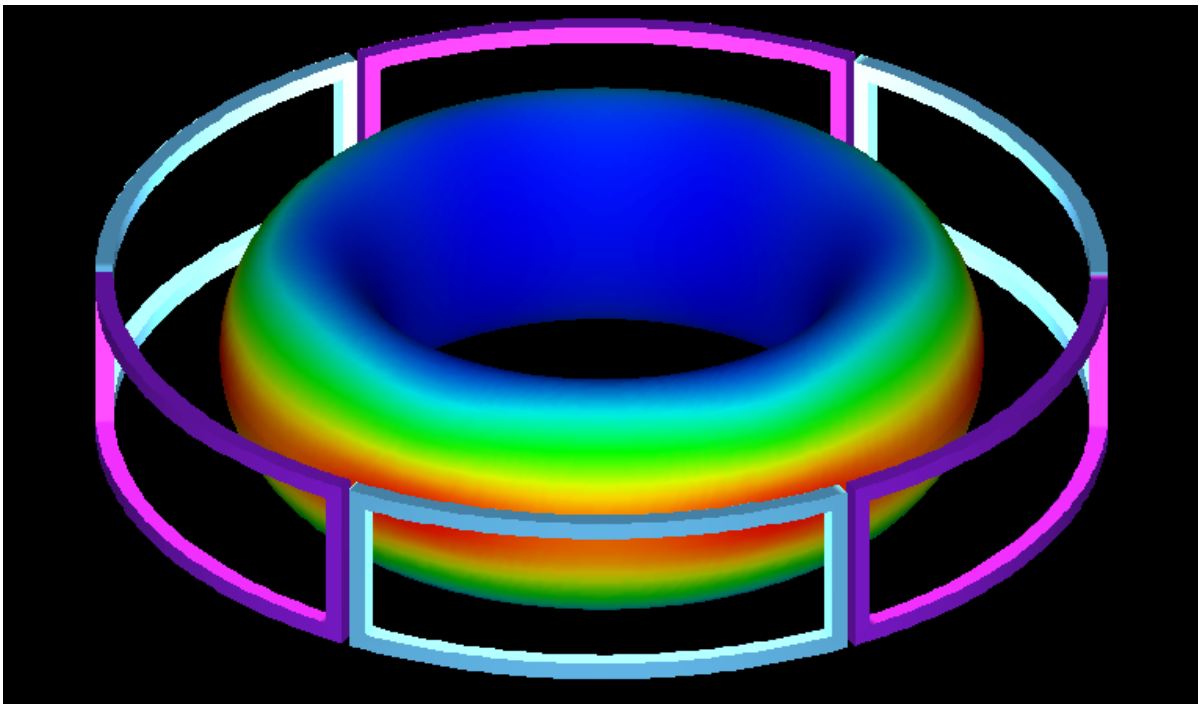

Fig. 9: Helical coils and plasma.

2.3.2 AUXILIARY COILS

The stellarator W7-X uses additional planar coils [5], so-called auxiliary coils, for the variation of the rotational transform. Separate adjustment of the currents in the coils allows the introduction of a vertical field to shift the magnetic axis.

W7-X auxiliary coils

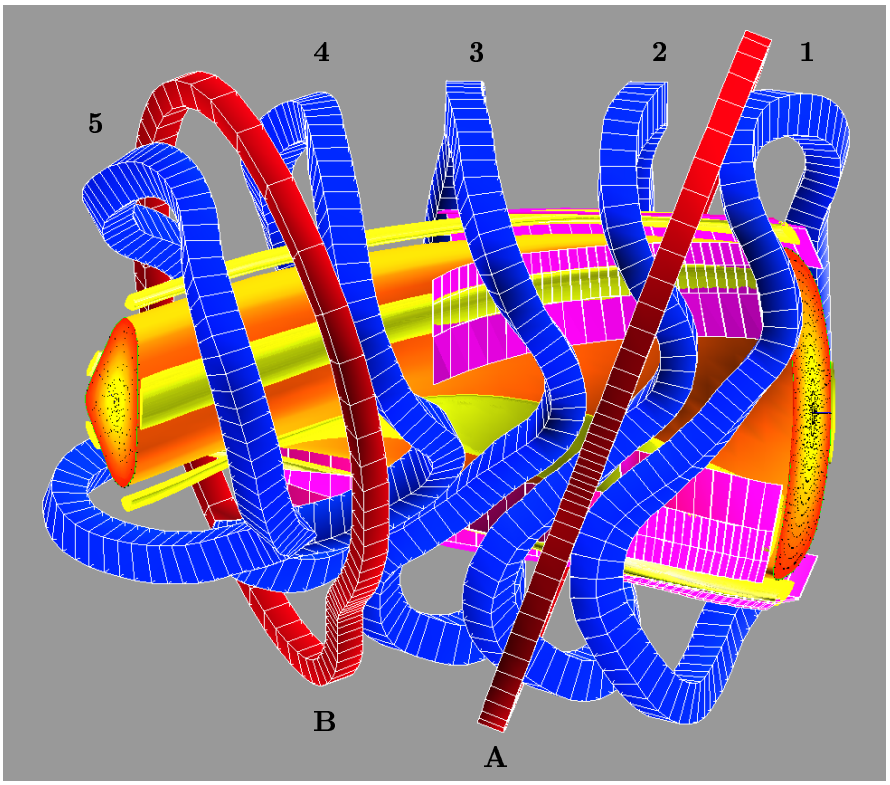

Fig. 10 Three-dimensional representation of the plasma tube (orange), the modular coils 1-5 (blue) and the auxiliary coils A and B (reddish brown) for half a period. The triangular cross-section on the left side and the bean-shaped cross-section on the right side include Poincaré plots of closed magnetic surfaces. Furthermore, the five islands of the standard case (yellow) and the proposed divertor and baffle plates (pink) are shown.

W7-X has four auxiliary coils per period, that is, 20 coils in total. Because of the stellarator symmetry and the five periods, the 20 coils are composed of only two different call types called A and B.

3. COMPUTATION OF THE MAGNETIC FIELD

3.1 DEFINITION OF THE GRID

The magnetic field has to be provided on discrete grid points for the succeeding codes (GOURDON, VMEC/NEMEC and MFBE). The grid has to cover the relevant region, that is, the plasma region and the boundary region up to the plasma facing components. Its resolution has to be sufficiently high to guarantee results independent of its discreteness. The grid plotted in Fig. 11 is chosen as cylindrical box satisfying the first requirement. The box is centred around the coordinates (R_0, Z_0). The half side lengths of the box are given by ΔR and ΔZ. Since R_0, Z_0, ΔR, and ΔZ do not vary in toroidal direction, it has to be made sure that the box fits for all toroidal cross-sections in case of three-dimensional configurations. To satisfy the second requirement the box has to be divided into a sufficient number of grid points N_R, N_Z, and N_φ.

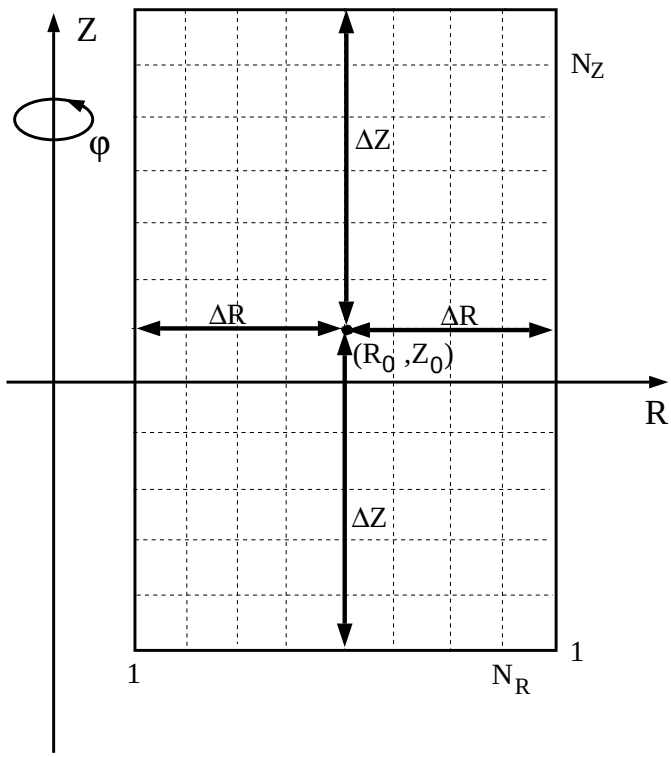

Fig. 11: Toroidal cross-section of the grid. The magnetic field is computed for N_R grid points in radial direction, N_φ grid points in toroidal direction and N_Z grid points in Z-direction.

3.2 BIOT-SAVART'S LAW

A coil is approximated by one or several infinitely thin conductor filaments. Each filament consists of straight pieces. Let N be the number of straight conductor pieces then the magnetic field produced by the filament is given by

$$\mathbf{B}(\mathbf{r}) = \sum_{\mathrm{i}}^{\mathrm{N}} \mathbf{B}^{\mathrm{i}}(\mathbf{r}) \tag{11}$$

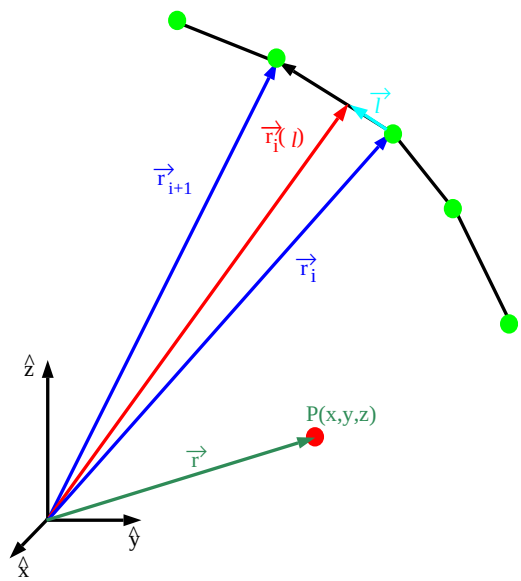

Fig. 12 Straight conductor pieces (black lines between green dots).

The magnetic field, $\mathbf{B}^{\mathrm{i}}$, produced by a single conductor piece at the point, $P(x,y,z)$, is determined by

Biot-Savart's law:

$$\mathbf{B}^{\mathrm{i}}(\mathbf{r}) = \frac{\mu_0}{4\pi} I_{\mathrm{i}} \int_0^1 \frac{\mathbf{k} \times (\mathbf{r} - \mathbf{r}_{\mathrm{i}}(l))}{|\mathbf{r} - \mathbf{r}_{\mathrm{i}}(l)|^3} |\mathbf{r}_{\mathrm{i}+1} - \mathbf{r}_{\mathrm{i}}| dl \tag{12}$$

with the unit vector, $\mathbf{k}$,

$$\mathbf{k} = \frac{\mathbf{r}_{\mathrm{i}+1} - \mathbf{r}_{\mathrm{i}}}{|\mathbf{r}_{\mathrm{i}+1} - \mathbf{r}_{\mathrm{i}}|} \tag{13}$$

pointing in the direction of the straight conductor line, and

$$\mathbf{r}_{\mathrm{i}}(l) = \mathbf{r}_{\mathrm{i}} + \mathbf{l} = \mathbf{r}_{\mathrm{i}} + l(\mathbf{r}_{\mathrm{i}+1} - \mathbf{r}_{\mathrm{i}}) \tag{14}$$

Analytical integration of Eq. (12) yields

$$\mathbf{B}^{\mathrm{i}}(\mathbf{r}) = \frac{\mu_0}{4\pi} I_{\mathrm{i}} \cdot \left((\mathbf{r} - \mathbf{r}_{\mathrm{i}}) \times (\mathbf{r} - \mathbf{r}_{\mathrm{i}+1}) \right)$$

$$\cdot \frac{|\mathbf{r} - \mathbf{r}_{\mathrm{i}}| + |\mathbf{r} - \mathbf{r}_{\mathrm{i}+1}|}{\left(|\mathbf{r} - \mathbf{r}_{\mathrm{i}}||\mathbf{r} - \mathbf{r}_{\mathrm{i}+1}| + (\mathbf{r} - \mathbf{r}_{\mathrm{i}})(\mathbf{r} - \mathbf{r}_{\mathrm{i}+1}) \right) \cdot |\mathbf{r} - \mathbf{r}_{\mathrm{i}}||\mathbf{r} - \mathbf{r}_{\mathrm{i}+1}|} \tag{15}$$

The explicit expressions of the first derivatives of the magnetic field are given in Appendix B1. The magnetic field and its first derivatives are needed in cylindrical co-ordinates. The co-ordinate transformation is given in Appendix B2. If the magnetic field is stellarator symmetric, it has to be computed for half a period only, while the field for the whole period is constructed using the symmetry relations listed in Appendix B3.

4. USE Of THE VACFIELD CODE

4.1 CODE STRUCTURE

The VACFIELD code is written in FORTRAN 90 using free allocation of arrays and free format. The source code can be transformed into a scalar or a parallelized version. The scalar version works on IBM workstations and on PCs with LINUX software. The parallelized version uses the MPI communication library and is available for IBM Regatta supercomputers and LINUX clusters.

The directory of the VACFIELD code has the following structure:

```
                              vacfield
                                 |
 ________________________________|____________________________________
 |     |        |        |      |        |         |        |       |
 |     |        |        |      |        |         |        |       |
src src_scal src_para src_split |     exe_ibm   exe_linux input     |
                                 |                                   |
                                 |                                   |
                  ______________|_________________                  |
                  |       |            |         |                  |
                  |       |            |         |                  |
              obj_ibm obj_ibm_para obj_linux obj_linux_para         |
                                                                    |
                                                                    |
                                                 ___________________|
                                                 |
                                                 |
                                               coils
                                                 |
                                        _________|_________
                                        |        |        |
                                        |        |        |
                                       AUG     W7-X      HSR
```

The source code is in subdirectory **src**. Individual program lines which are only used in the parallel code version are marked with **$P**, while several lines, which are special for the parallel or scalar code version, are included in if-statetments of the following forms:

```
$IF (PARA) THEN
! --- initialize MPI
      call init_MPP_environment()
      nproz = npes
      npid  = pid
$ENDIF


$IF (SCAL) THEN
      nproz = 1
      npid  = 0
$ENDIF
```

Routines in the subdirectory **src_split** split the source code into a scalar code stored in **src_scal** and a parallelized code stored in **src_par**. The makefiles for compiling the two code versions on various computers are in the corresponding subdirectories **obj_ibm** (IBM work station), **obj_ibm_para** (IBM Regatta supercomputer), **obj_linux** and **obj_linux_para** (LINUX cluster). The subdirectories **exe_ibm** and **exe_linux** contain executables and script files for the IBM and LINUX systems. Examples of standard input files for tokamak and stellarator devices are given in subdirectory **input**, while the coil geometries for ASDEX Upgrade (AUG), Wendelstein 7-X (W7-X) and the HELIAS reactor (HSR) are in the subdirectories **coils/AUG**, **coils/W7-X** and **coils/HSR**.

4.1.1 SOURCE CODE

The VACFIELD code contains the following main program, modules and subroutines.

main program:

vacfield.f90	main program

modules:

mod_add.f90	additional coils: coil geometry and currents
mod_bfield.f90	grid geometry and magnetic field
mod_const.f90	physical constants and working parameters
mod_corr.f90	correction coils: coil geometry and currents
mod_main.f90	main field coils: coil geometry and currents
mpp_functions.f90	parallelization: MPP job environment

subroutines: reading of the input

read_auxcoil.f90	auxiliary coils
read_input.f90	standard input file
read_helcoil.f90	helical coils
read_modcoil.f90	modular coils
read_polcoil.f90	poloidal field coils
read_sadcoil.f90	saddle coils
read_torcoil.f90	toroidal field coils

subroutines: computation of the magnetic field

compute.f90	total magnetic field
auxcoil.f90	field of the auxiliary coils
helcoil.f90	field of the helical coils
modcoil.f90	field of the modular coils
polcoil.f90	field of the poloidal field coils
sadcoil.f90	field of the saddle coils
toraxsy.f90	axisymmetric approximation of the toroidal field
torcoil.f90	field of the toroidal field coils
bfield.f90	transformation of the magnetic field and its first derivatives into cylindrical co-ordinates
biotsav.f90	Biot-Savart's law: magnetic field in Cartesian co-ordinates on a grid point
biotsavd.f90	Biot-Savart's law: magnetic field and its first derivatives in Cartesian co-ordinates on a grid point

subroutines: writing of the magnetic field output

out_mfbe.f90	magnetic field input to the MFBE and GOURDON codes
out_vmec.f90	magnetic field input to the VMEC/NEMEC code

4.1.2 CODE SPLITTING

The subdirectory **src_split** contains the tools for splitting the source code into a scalar and a parallel code version.

split.f90	FORTRAN code which splits the source code (**src**) into a scalar (**src_scal**) and a parallel (**src_para**) code version
source	total list of routines in subdirectory **src**
split_ibm.e	script for executing program **split.f90** on an IBM computer
split_linux.e	script for executing program **split.f90** on a PC or a LINUX cluster

If the scalar and parallel code versions already exist, but subroutines of the source code have been modified, it is recommendable to compile only the modified routines. Since the makefiles (see next section) compile all routines with a date newer than that of already existing object files, only the modified routines are to be rewritten in the subdirectories **src_scal** and **src_para**. For this purpose, the file **source_corr** and the scripts **split_corr_ibm.e** and **split_corr_linux.e** are available.

4.1.3 MAKEFILES

The subdirectories **obj_ibm**, **obj_ibm_para**, **obj_linux** and **obj_linux_para** contain makefiles and object codes for IBM workstations, IBM Regatta supercomputers, PCs and LINUX clusters. They generate the executables **VACFIELD_IBM** and **VACFIELD_IBM_PARA** in subdirectory **exe_ibm**, and **VACFIELD_LINUX** and **VACFIELD_LINUX_PARA** in subdirectory **exe_linux**.

In the following, compiler and loader options used in the makefiles are listed.

Makefile for IBM workstations (scalar code)

FORTRAN compiler:	xlf90
compiler flags:	-qautodbl=dbl4 -c -03 -ev -qsuffix=cpp=f90
loader:	xlf90

Makefile for IBM Regatta supercomputers (parallelized code)

fortran compiler:	mpxlf90_r
compiler flags:	-qautodbl=dbl4 -c -03 -qsuffix=cpp=f90
loader:	mpxlf90_r

Makefile for PCs and LINUX clusters (scalar code)

FORTRAN compiler:	f95i
compiler flags:	-c -v 8.1 -w -FR -r8 -O3 -ip -tpp7 -xW
loader:	f95i

Makefile for LINUX clusters (parallelized code)

FORTRAN compiler:	mpif95i
compiler flags:	-c -v 8.1 -w -FR -r8 -O3 -ip -tpp7 -xW
loader:	mpif95i

4.1.4 EXECUTABLES AND SCRIPTS

The executables of the code and the scripts for its interactive execution are given in the directories **exe_ibm** and **exe_linux**.

directory exe_ibm (IBM workstations and IBM Regatta supercomputer)

VACFIELD_IBM	executable of the scalar code
VACFIELD_IBM_PARA	executable of the parallelized code
vacfield_ibm.e	script for executing the scalar code
vacfield_ibm_para.e	script for executing the parallelized code

directory exe_linux (PCs and LINUX clusters)

VACFIELD_LINUX	executable of the scalar code
VACFIELD_LINUX_PARA	executable of the parallelized code
vacfield_linux.e	script for executing the scalar code
vacfield_linux_para.e	script for executing the parallelized code

Note, the code is parallelized in Z-direction, that is, the number of grid points, N_Z (see Sect. 3.1 and Sect. 4.2.1), has to be a multiply of the number of processors chosen in the scripts **vacfield_ibm_para.e** and **vacfield_linux_para.e**. For a typical, three-dimensional grid (compare Sect. 5.1) the computational time is less than 15 minutes using 16 processors. That is, in general it is not necessary to submit a batch job.

4.2 INPUT

The VACFIELD code uses SI units, that is, all input and output quantities are given in these units. The code needs several input files. The input quantities are read in the subroutines **read_input.f90, read_auxcoil.f90**, etc..

4.2.1 STANDARD INPUT

The standard input file contains names of further input and output files, symmetry and grid parameters, and coil currents.

Example of a standard input file

```
output:     'out_vac_axi_cliste_lb'
out_mfbe:   'vacfield_mfbe_axi_cliste_lb'
type_mfbe:  'binary'
out_vmec:   'vacfield_vmec_axi_cliste_lb'
type_vmec:  'binary'
symmetry:   'axisymmetry'
derivative: 'no'
grid:       nf    nr    nz   np
             1   100    128   1
            centre (r0,z0) half width (dr,dz)
              r0      z0      dr      dz [m]
            1.625   0.000   0.975   1.500
main_coils: 'axisymmetric'
main_input: 'none'
            ncoil_main
                 1
current:    j_main   [MA]
            -22.918
fm(i):      (i=1,...,ncoil_main)
               1.00
corr_coils: 'poloidal field coils'
corr_input: '.../vacfield/coils/AUG/polcoils_cliste'
            ncoil_corr
               13
            type_corr(i)   fc(i)  [MA]
            IV1o           1.306
            IV1u           0.742
            IV2o          -0.982
            IV2u          -0.309
            IV3o           0.001
            IV3u          -0.115
            ICoIo         -0.026
            ICoIu         -0.019
            Ipslon         0.029
            Ipslun        -0.018
            IHO2od         0.449
            IHO2ud         0.449
            IOH            5.354
add_coils:  'none'
add_input:  'none'
            ncoil_add
```

```
                1
fa(i):       (i=1,...,ncoil_add)    [MA]
              0.0
```

List of variables:

input and output file names

output	character∗80	name of the standard output file
out_mfbe	character∗80	magnetic field input to the MFBE and GOURDON codes
type_mfbe	character∗40	type of the file format
	ascii	
	binary	
out_vmec	character∗80	mag. field input to the VMEC/NEMEC code
type_vmec	character∗80	type of the file format
	ascii	
	binary	

symmetry and derivatives of the magnetic field

symmetry	character∗80	symmetry of the magnetic field
	none	
	up-down axisymmetry	
	axisymmetry	
	stellarator symmetry	
derivative	character∗3	computation of the first derivatives
	yes	
	no	

magnetic field grid (for details see Sect. 3.1)

nf	integer	number of toroidal grid points per period
nr	integer	number of grid points in R-direction
nz	integer	number of grid points in Z-direction
np	integer	number of periods
r0	real	R-co-ordinate of the centre of the grid
z0	real	Z-co-ordinate of the centre of the grid
dr	real	half width of the grid in R-direction
dz	real	half width of the grid in Z-direction

main field coils

main_coils	character∗80	type of the main field coils
	none	no main field
	axisymmetric	axisymmetric approximation of the main field, Eq.(1)
	toroidal field coils	tokamak main field coils
	modular coils	stellarator main field coils
main_input	character∗80	input file name of the main field coils
ncoil_main	integer	number of coil currents
j_main	real	average current per coil given in [MA]
fm(i)	real	variations of the coil currents with respect to *j_main* (i=1,...,ncoil_main)

correction coils

corr_coils	character∗80	type of the correction coils
	none	no correction field
	poloidal field coils	tokamak correction coils
	saddle coils	stellarator correction coils
corr_input	character∗80	input file name of the correction coils
ncoil_corr	integer	number of coil currents
type_corr(i)	character∗10	types of correction coils (i=1,...,ncoil_corr)
fc(i)	real	coil currents (i=1,...,ncoil_corr) given in [MA]

Note, depending on the types of the poloidal field coils of AUG, the coil currents, fc(i), are the total coil currents (input files: **polcoils_simple** and **polcoils_cliste**) or the currents per winding (input file: **polcoils_hpz**).

additional coils

add_coils	character∗80	type of the additional coils
	none	no additional coils
	helical coils	helical coils for tokamaks
	auxiliary coils	stellarator auxiliary coils
add_input	character∗80	input file name of the additional coils
ncoil_add	integer	number of additional currents
fa(i)	real	coil currents (i=1,...,ncoil_add) given in [MA]

4.2.2 MAIN FIELD COILS

Depending on the device, the main field is generated by toroidal field coils or modular coils. The input data of ASDEX Upgrade toroidal field coils have the following form.

Example of an input file: toroidal field coils

```
           ASDEX Upgrade toroidal field coils
           ----------------------------------
main_symmetry:              'stellarator symmetry'
number of possible periods:  np_mpos
                               5
possible period numbers:     mpo(i=1,np_mpos)
                               1   2   4   8   16
   nspul_main    iseg_main   np_main
       1            10         16
  r0cs      z0cs      racs      alfa0     alfa1   ncs
   [m]       [m]       [m]     [grad]    [grad]
1.11923   0.00000   1.86447     0.000    18.916    9
1.21180   0.03172   1.76661    18.916    36.860    8
1.34287   0.13000   1.60278    36.860    54.788    7
1.46344   0.30084   1.39369    54.788    72.755    6
1.52688   0.50521   1.17969    72.755    90.716    5
1.52438   0.70472   0.98016    90.716   108.732    5
1.47259   0.85745   0.81890   108.732   126.743    4
1.39916   0.95581   0.69615   126.743   144.829    3
1.33694   0.99965   0.62003   144.829   162.886    3
1.29987   1.01106   0.58125   162.886   180.000    3
```

List of variables:

coil symmetry

main_symmetry	character*60	coil symmetry
	none	
	stellarator symmetry	
np_mpos	integer	number of possible periods
mpo(i)	integer	possible period numbers (i=1,...,np_mpos)

coil geometry (for details see Sect. 2.1.2)

nspul_main	integer	number of coils per period
iseg_main	integer	number of coil segments
np_main	integer	number of periods
r0cs(i)	real	*R*-co-ordinate of the circle centre
z0cs(i)	real	*Z*-co-ordinate of the circle centre
racs(i)	real	radius of the circle
alfa0(i)	real	lower poloidal boundary of the circle segment
alfa1(i)	real	upper poloidal boundary of the circle segment
ncs(i)	integer	number of straight pieces per circle segment (i=1,...,iseg_main)

Input data of modular stellarator coils have the following form:

Example of an input file: modular coils

```
            Wendelstein 7-X modular field coils
            -----------------------------------
main_symmetry:              'stellarator symmetry'
number of possible periods:  np_mpos
                               2
possible period numbers:     mpo(i=1,np_mpos)
                               1   5
   nspul_main    iseg_main   np_main
     10             97          5
        x [m]           y [m]             z [m]           I [MA]
   6.842620711E+00   4.311918695E-01   1.744954334E-02  -1.000000000E+00
   6.839498568E+00   4.265082904E-01   1.063739981E-01  -1.000000000E+00
         :                 :                 :                 :
         :                 :                 :                 :
   6.842620711E+00   4.311918695E-01   1.744954334E-02   0.000000000E+00
   6.643640420E+00   1.378705287E+00   2.786784824E-03  -1.000000000E+00
   6.639687437E+00   1.365792034E+00   9.012406132E-02  -1.000000000E+00
         :                 :                 :                 :
         :                 :                 :                 :
   6.643640420E+00   1.378705287E+00   2.786784824E-03   0.000000000E+00
   6.363713956E+00   2.128162379E+00   3.632685538E-02  -1.000000000E+00
         :                 :                 :                 :
```

List of variables:

coil symmetry

main_symmetry	character∗60	coil symmetry
	none	
	stellarator symmetry	
np_mpos	integer	number of possible periods
mpo(i)	integer	possible period numbers (i=1,np_mpos)

coil geometry (see Sect. 2.1.3)

nspul_main	integer	number of coils per period
iseg_main	integer	number of segments per coil
np_main	integer	number of periods
x(i)	real	*x*-co-ordinate of the current filament
y(i)	real	*y*-co-ordinate of the current filament
z(i)	real	*z*-co-ordinate of the current filament
I(i)	real	unit current (note the sign).
	real	(i=1,..,iseg_main·nspul_main)

4.2.3 CORRECTION COILS

In the VACFIELD code two types of correction coils are implemented, namely ASDEX Upgrade poloidal field coils and W7-X saddle coils.

Example of an input file: AUG poloidal field coils

```
            ASDEX Upgrade poloidal field coils (CLISTE format)
            --------------------------------------------------
corr_symmetry:              'axisymmetry'
 ntotal_corr iseg_corr  ngroup_corr
  896         361          13
 ntype_corr     type_corr  ntotal_turns
   6            IV1o           93
   6            IV1u           93
   6            IV2o           86
   6            IV2u           86
```

```
  2            IV3o           28
  2            IV3u           28
  5            IColo           5
  5            ICoIu           5
 12            Ipslon          1
 12            Ipslun          1
 80            IHO2od         81
 80            IHO2ud         81
674            IOH           682
-----------------------------------------------------------------
 IV1o     R          Z        Turns
-----------------------------------------------------------------
         1.38360   2.27157  17.50000
         1.38360   2.44472  17.50000
         1.59795   2.27157  15.50000
         1.59795   2.44472  15.50000
         1.95720   2.27157  13.50000
         1.95720   2.44472  13.50000
-----------------------------------------------------------------
 IV1u     R         Z         Turns
-----------------------------------------------------------------
         1.38160  -2.44495  17.50000
         1.38160  -2.27165  17.50000
         1.59555  -2.44495  15.50000
          :         :         :
          :         :         :
          :         :         :
```

List of variables:

coil symmetry

corr_symmetry	character∗60 axisymmetry up-down axisymmetry	coil symmetry

coil geometry (for details see Sect. 2.2.1)

ntotal_corr	integer	total number of coil filaments
iseg_corr	integer	number of segments per coil
ngroup_corr	integer	number of coil types

ntype_corr(i)	integer	number of coil filaments per coil type
type_corr(i)	character∗10	coil type
ntotal_turns(i)	integer	total number of windings per coil type (i=1,...,ngroup_corr)
R(j)	real	*R*-co-ordinate of the filament centre
Z(j)	real	*Z*-co-ordinate of the filament centre
turns(j)	real	winding number of the coil filament (j=1,...,ntype_corr(i))

The input file format of the W7-X saddle coils is equal to the W7-X modular coils (Sect. 4.2.2).

4.2.4 ADDITIONAL COILS

Two types of additional coils are implemented in the VACFIELD code.

An example of helical coils is given below. These helical coils are only used for numerical simulations of ASDEX Upgrade type plasma configurations, but the coils are not installed in ASDEX Upgrade.

Example of an input file: helical coils

```
            ASDEX Upgrade helical coils
            ---------------------------
add_symmetry:                'none'
number of possible periods:  np_apos
                               2
possible period numbers:     apo(i=1,np_apos)
                               1    3
   nspul_add     np_add
      2             3
   phi1_hel   phi2_hel   nphi_hel
     0.5        59.5      60
   r11    z11    r22    z22
   2.77   0.5   2.77   -0.5
```

List of variables:

coil symmetry

add_symmetry	character∗60	coil symmetry
	none	
	stellarator symmetry	
np_apos	integer	number of possible periods
apo(i)	integer	possible period numbers (i=1,...,np_apos)

coil geometry (see also Sect. 2.3.1)

nspul_add	integer	number of coils per period
np_add	integer	number of periods
phi1_hel	real	lower toroidal boundary of one coil
phi2_hel	real	upper toroidal boundary of one coil
nphi_hel	real	number of toroidal coil segments
r11	real	radial co-ord. of the upper toroidal coil segment
z11	real	Z-co-ordinate of the upper toroidal coil segment
r22	real	radial co-ord. of the lower toroidal coil segment
z22	real	Z-co-ordinate of the lower toroidal coil segment

The input file format of the W7-X auxiliary coils is equal to the W7-X modular coils (see Sect. 4.2.2).

4.3 OUTPUT

The VACFIELD code produces several output files, namely, the standard output, a possible error output, and the magnetic field input to the MFBE and GOURDON codes, and/or the VMEC/NEMEC code.

4.3.1 STANDARD OUTPUT

The standard output file contains the input parameters of all used input files, as well as some computed values of the magnetic field (and its first derivatives) for specified co-ordinate points.

4.3.2 VACUUM MAGNETIC FIELD INPUT TO THE MFBE AND GOURDON CODES

The vacuum magnetic field input to the MBFE and GOURDON codes is an ascii or a binary file (real double precision data).

List of variables:

Dimensions of the vacuum field

enf	real	number of toroidal plans per period
	enf =1	axisymmetric field
enr	real	number of grid points in *R*-direction
enz	real	number of grid points in *Z*-direction
ena	real	number of components of the magnetic field (and its first derivatives)
enp	real	number of periods
enfd	real	number of toroidal plans for which the magnetic field is computed
	enfd= nint(enf)/2+1	stellarator-symmetric field
	enfd = enf	asymmetric field

Note, in order to avoid difficulties with different integer lengths on different computers, these quantities are defined as real variables in read and write instructions. They are transformed into integer variables inside the code.

Boundaries of the grid (compare Fig. 11)

r00	real	*R*-co-ordinate of the centre of the grid
z00	real	*Z*-co-ordinate of the centre of the grid
dr0	real	half width of the grid in *R*-direction
dz0	real	half width of the grid in *Z*-direction

Vacuum magnetic field produced by external coils

bb(1,k,l)	real	B_φ-component
bb(2,k,l)	real	B_R-component
bb(3,k,l)	real	B_Z-component
bb(4,k,l)	real	$\partial B_\varphi/\partial\varphi$
bb(5,k,l)	real	$\partial B_\varphi/\partial R$
bb(6,k,l)	real	$\partial B_\varphi/\partial Z$
bb(7,k,l)	real	$\partial B_R/\partial\varphi$
bb(8,k,l)	real	$\partial B_R/\partial R$
bb(9,k,l)	real	$\partial B_R/\partial Z$
bb(10,k,l)	real	$\partial B_Z/\partial\varphi$
bb(11,k,l)	real	$\partial B_Z/\partial R$
bb(12,k,l)	real	$\partial B_Z/\partial Z$

Note, there are $enfd$ blocks $bb(i,k,l)$ written ($1 \le i \le ena$, $1 \le k \le enr$ (R-direction) and $1 \le l \le enz$ (Z-direction)). For more details see write statements in subroutine writ_mfbe.f90.

4.3.3 VACUUM MAGNETIC FIELD INPUT TO THE VMEC/NEMEC CODE

The vacuum magnetic field input to the VNEC/NEMEC code is a binary (real double precision data) or an ascii file.

List of variables:

Dimensions of the vacuum field

anr0b	real	number of grid points in R-direction
anz0b	real	number of grid points in Z-direction
anp0b	real	number of toroidal plans per period
	anp0b =1	axisymmetric field
anfper0	real	number of periods

Boundaries of the grid (see Fig. 11)

rminb	real	R-co-ordinate of the left grid boundary
zminb	real	Z-co-ordinate of the lower grid boundary
rmaxb	real	R-co-ordinate of the right grid boundary
zmaxb	real	Z-co-ordinate of the upper grid boundary

Vacuum magnetic field produced by external coils

bb(i,1)	real	B_R-component
bb(i,2)	real	B_Z-component
bb(i,3)	real	B_φ-component

with $1 \leq i \leq anr0b \cdot anz0b \cdot anp0b$. For more details see write statements in routine writ_vmec.f90.

4.3.4 ERROR OUTPUT

Most of the errors resulting from wrong input parameters are recognized by the code. Error messages are be written into the error output file and the execution of the code is terminated. Below a list of examples of possible error messages is given (this list is not complete):

wrong input or output file name

```
****************************************************
* ERROR: standard output file could not be opened *
* STOP in subroutine READ_INPUT                   *
****************************************************
```

wrong file format

```
****************************************************
* ERROR: no valid file format for type_mfbe       *
* STOP in subroutine READ_INPUT                   *
****************************************************
```

wrong kind of coils

```
****************************************************
* ERROR: no valid kind of main coils              *
* STOP in subroutine READ_INPUT                   *
****************************************************
```

wrong number of periods

```
****************************************************
* ERROR: np not compatible with coils geometry    *
* STOP in subroutine READ_TORCOIL                 *
****************************************************
```

5. ACCURACY TESTS

5.1 W7-X VACUUM MAGNETIC FIELD

The modular coils of the advanced helical W7-X stellarator produce vacuum magnetic fields which already exhibit closed magnetic flux surfaces. Field lines forming closed surfaces can be traced over arbitrarily lengths. Therefore, such a magnetic configuration is used for the accuracy tests described in this section.

The magnetic field is computed with and without first derivatives on grids with various numbers of grid points, (N_φ,N_R,N_Z), in toroidal, radial and Z-directions. The various cases are listed below.

case	N_φ	N_R	N_Z	first derivatives
1	30	32	32	no
2	62	64	64	no
3	126	128	128	no
4	30	32	32	yes
5	62	64	64	yes
6	126	128	128	yes

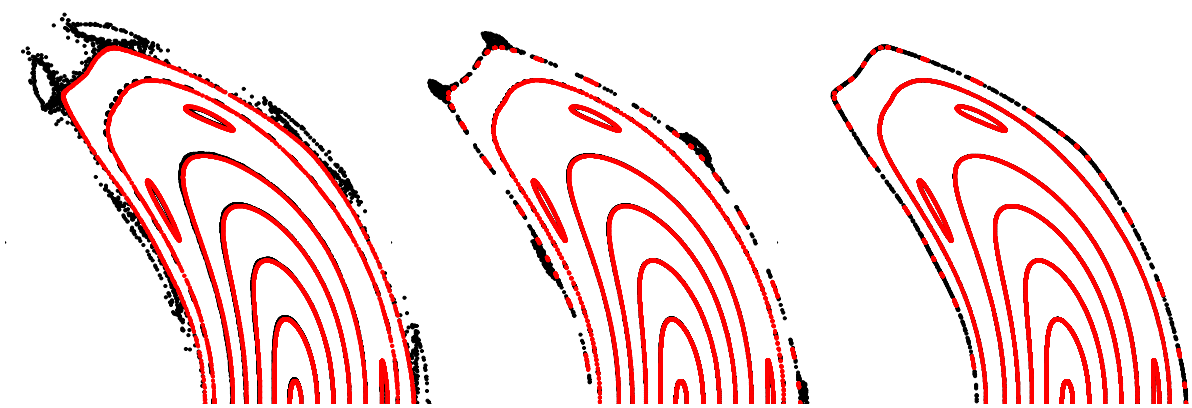

Fig. 13: Poincaré plots showing the upper halves of bean-shaped cross-sections ($\varphi = 0^o$). Field line tracing has been performed with (red dots) and without (black dots) taking into account the first derivatives of the magnetic field, but using the same starting points. Furthermore, various grids have been used for the computations: **left:** low number (case 1,4), **middle:** intermediate number (case 2,5), **right:** high number of grid points (case 3,6).

After computing the magnetic field with the VACFIELD code, the GOURDON code is used for tracing field lines and computing their rotational transform values. In Fig. 13 the resulting magnetic field structures computed with and without first derivatives and different numbers of grid points are compared. Figure 14 shows an enlargement of a part of the last surface inside the inner islands (see Fig. 13). Finally, in Fig. 15 the inner part of the rotational transform profile is plotted for the cases (1-4,6).

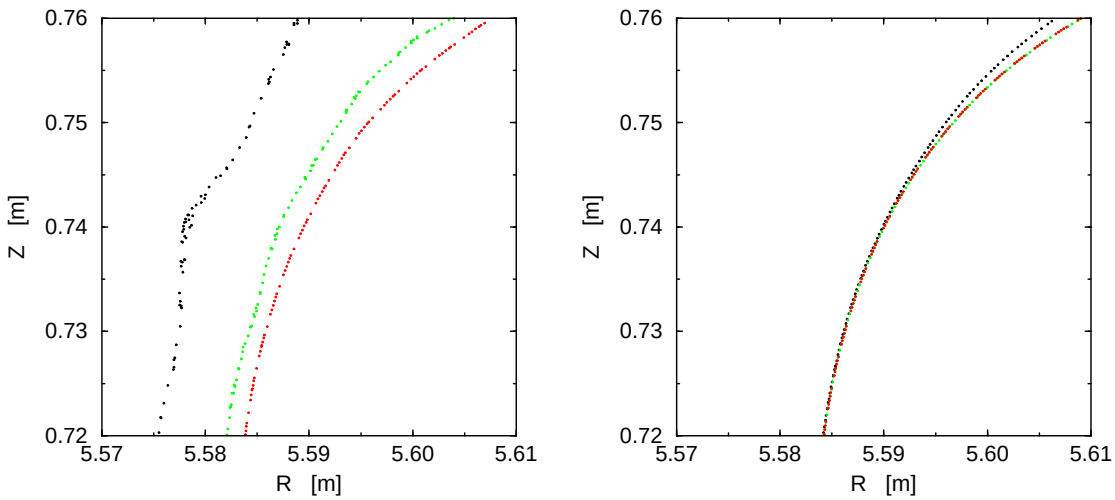

Fig. 14: Single field line traced without (**left**) and with (**right**) using the first derivatives. The results are shown for three resolutions of the grid: cases 1,4 (black dots), cases 2,5 (red dots), case 3,6 (green dots).

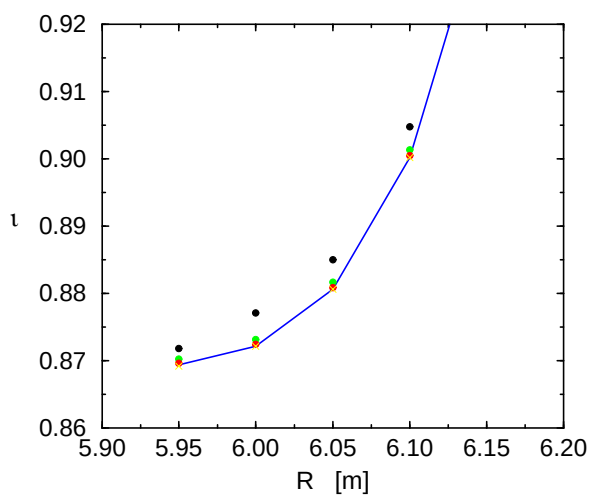

Fig. 15: Inner part of the rotational transform profile for various cases: case 1 (black dots), case 2 (green dots), case 3 (red dots), case 4 (yellow crosses), case 6 (blue line). The values of case 5 have been neglected because they agree with the results of case 6 with high accuracy.

The computations made without first derivatives are very sensitive to the number of grid points. However, including the first derivatives leads to satisfactory results even for a low resolution

grid. For the high resolution grid the results obtained with and without first derivatives agree very well. That is, a sufficient numerical accuracy is either obtained by including the first derivatives or by using a high resolution grid. The figures also demonstrate that for complex magnetic structures (e.g. separatrices, island remnants, stochastic field lines) a higher numercial accuracy (more grid points, use of first derivatives) is necessary than for simpler ones (e.g. smooth nested surfaces in the plasma core).

5.2 AUG FREE-BOUNDARY EQUILIBRIUM

The accuracy of a computed magnetic field also depends on the geometrical description of the coils. Extended coils have to be represented by several current filaments. There are two kinds of descriptions in use for the ASDEX Upgrade poloidal field coils: a.) a very detailed representation consisting of 896 coil filaments (input file: **polcoils_cliste** (see Appendix A2)), and b.) one more compact representation consisting of 128 filaments (input file: **polcoils_hpz** (see Appendix A2)).

For comparing both coil sets, free-boundary finite-β equilibria of an AUG configuration are computed with the VMEC/NEMEC code using vacuum magnetic fields computed with the coil sets **polcoils_hpz** and **polcoils_cliste**. Resulting equilibrium quantities are compared below.

equilibrium quantities		polcoils_hpz	polcoils_cliste	difference [%]
R_{mag}	[m]	1.797	1.794	0.13
Z_{mag}	[m]	0.043	0.039	0.19
R_{in}	[m]	1.162	1.160	0.12
R_{out}	[m]	2.177	2.175	0.14
V	[m^3]	13.04	13.02	0.22
E_{kin}	[MJ]	0.388	0.387	0.23
I_p	[MA]	0.667	0.668	0.15
$<\beta>$	[%]	0.615	0.613	0.33

These quantities are: co-ordinates of the magnetic axis (R_{mag}, Z_{mag}), inner and outer radial co-ordinate of the plasma boundary (R_{in}, R_{out}), plasma volume (V), plasma energy (E_{kin}), toroidal plasma current (I_p), and volume averaged plasma beta ($<\beta>$). All quantities agree very well, that is, 128 coil filaments are suffficient for representing the AUG poloidal field coils.

ACKNOWLEDGEMENTS

We hereby would like to thank J. Kißlinger for providing the W7-X and HSR coil data, and Fig. 8 in Sect. 2.2.2. We also would like to thank P. Martin and H.-P. Zehrfeld for the AUG coil data.

References

[1] Hirshman, S.P. and Lee, D.K., Comput. Phys. Commun. **39** (1986) 161.

[2] Hirshman, S.P., van Rij, W.I., Merkel, P., Comput. Phys. Commun. **43** (1986) 143.

[3] Strumberger, E., Nuclear Fusion **37** (1997) 19.

[4] Strumberger, E., Merkel P. Schwarz E. and Tichmann C., Laboratory Report IPP 5/100, Garching 2002. http://www.ipp.mpg.de/netreports/ipp-report_5_100.ps.

[5] Beidler, C., et al., Fusion Technology **17** (1990) 148.

[6] Beidler, C.D. et al., Nuclear Fusion **41** (2001) 1759.

[7] Renner, H. et al., Nuclear Fusion **40** (2000) 1083.

[8] La Haye, R.J., Günter, S., Humphreys, D.A., Lohr, J., Luce, T.C., Maraschek, M.E., Petty, C.C., Prater, R., Scoville, J.T. and Strait, E.J., Phys. Plasmas **9** (2002) 2051.

A. APPENDIX: AVAILABLE COIL SETS

A.1 MAIN FIELD COILS

- tokamak: ASDEX Upgrade

path: ../coils/AUG/

torcoils	16 periodic configuration with one toroidal field coil per period (R_0 = 1.65 m, $a_0 \approx$ = 0.30)

- stellarator: W7-X

path: ../coils/W7-X/

mod_hs5v10u	five periodic configuration with 10 coils per period (R_0 = 5.5 m, a_0 = 0.55 m)

- stellarator reactor: W7-X

path: ../coils/HSR/

sp3v10nr96	three periodic configuration with 10 coils per period (R_0 = 18 m, a_0 = 2.1 m)
sp4v10nr96_m4.3	four periodic configuration with 10 coils per period (R_0 = 15 m, a_0 = 2.1 m)
sp5v10nr96_n1	five periodic configuration with 10 coils per period (R_0 = 22 m, a_0 = 2.0 m)
sp5v10nr96_n2	five periodic configuration with 10 coils per period (R_0 = 22 m, a_0 = 2.0 m)
sp5v10nr96_lsh	five periodic configuration with 10 coils per period (R_0 = 22 m, a_0 = 2.0 m, low shear)

A.2 CORRECTION COILS

- tokamak: ASDEX Upgrade

path: ../coils/AUG/

polcoils_simple	approximation of the poloidal field coils by single windings; without IOH coil
polcoils_cliste	representation of the poloidal field coils by 896 coil filaments
polcoils_hpz	representation of the poloidal field coils by 128 coil filaments

- stellarator: W7-X

path: ../coils/W7-X/

sweepsp-010402	two sweep coils in one period

A.3 ADDITIONAL COILS

- tokamak: ASDEX Upgrade

Note, helical field coils are not installed in AUG, but only used for numerical simulations.

path: ../coils/AUG/

helcoil_6	six helical field coils
helcoil_8	eight helical field coils

- stellarator: W7-X

path: ../coils/W7-X/

aux_hs5v10u	four auxiliary coils in one period

B. APPENDIX: BIOT-SAVART'S LAW

B.1 FIRST DERIVATIVES OF THE MAGNETIC FIELD

Using the definitions

$$f(\mathbf{r}) = \frac{|\mathbf{r}-\mathbf{r}_{\mathrm{i}}| + |\mathbf{r}-\mathbf{r}_{\mathrm{i+1}}|}{(|\mathbf{r}-\mathbf{r}_{\mathrm{i}}||\mathbf{r}-\mathbf{r}_{\mathrm{i+1}}| + (\mathbf{r}-\mathbf{r}_{\mathrm{i}})(\mathbf{r}-\mathbf{r}_{\mathrm{i+1}}))|\mathbf{r}-\mathbf{r}_{\mathrm{i}}||\mathbf{r}-\mathbf{r}_{\mathrm{i+1}}|} \tag{16}$$

and

$$\begin{aligned}\frac{\partial f(\mathbf{r})}{\partial x} = &\frac{-1}{(|\mathbf{r}-\mathbf{r}_{\mathrm{i}}||\mathbf{r}-\mathbf{r}_{\mathrm{i+1}}| + (\mathbf{r}-\mathbf{r}_{\mathrm{i}})(\mathbf{r}-\mathbf{r}_{\mathrm{i+1}}))|\mathbf{r}-\mathbf{r}_{\mathrm{i}}||\mathbf{r}-\mathbf{r}_{\mathrm{i+1}}|} \\ &\cdot\left(\frac{(x-x_{\mathrm{i}})|\mathbf{r}-\mathbf{r}_{\mathrm{i+1}}|}{|\mathbf{r}-\mathbf{r}_{\mathrm{i}}|^2} + \frac{(x-x_{\mathrm{i+1}})|\mathbf{r}-\mathbf{r}_{\mathrm{i}}|}{|\mathbf{r}-\mathbf{r}_{\mathrm{i+1}}|^2}\right) \\ &-\frac{(|\mathbf{r}-\mathbf{r}_{\mathrm{i}}| + |\mathbf{r}-\mathbf{r}_{\mathrm{i+1}}|)^2(|\mathbf{r}-\mathbf{r}_{\mathrm{i+1}}|(x-x_{\mathrm{i}}) + |\mathbf{r}-\mathbf{r}_{\mathrm{i}}|(x-x_{\mathrm{i+1}}))}{|\mathbf{r}-\mathbf{r}_{\mathrm{i}}|^2|\mathbf{r}-\mathbf{r}_{\mathrm{i+1}}|^2(|\mathbf{r}-\mathbf{r}_{\mathrm{i}}||\mathbf{r}-\mathbf{r}_{\mathrm{i+1}}| + (\mathbf{r}-\mathbf{r}_{\mathrm{i}})(\mathbf{r}-\mathbf{r}_{\mathrm{i+1}}))^2}\end{aligned} \tag{17}$$

$$\begin{aligned}\frac{\partial f(\mathbf{r})}{\partial y} = &\frac{-1}{(|\mathbf{r}-\mathbf{r}_{\mathrm{i}}||\mathbf{r}-\mathbf{r}_{\mathrm{i+1}}| + (\mathbf{r}-\mathbf{r}_{\mathrm{i}})(\mathbf{r}-\mathbf{r}_{\mathrm{i+1}}))|\mathbf{r}-\mathbf{r}_{\mathrm{i}}||\mathbf{r}-\mathbf{r}_{\mathrm{i+1}}|} \\ &\cdot\left(\frac{(y-y_{\mathrm{i}})|\mathbf{r}-\mathbf{r}_{\mathrm{i+1}}|}{|\mathbf{r}-\mathbf{r}_{\mathrm{i}}|^2} + \frac{(y-y_{\mathrm{i+1}})|\mathbf{r}-\mathbf{r}_{\mathrm{i}}|}{|\mathbf{r}-\mathbf{r}_{\mathrm{i+1}}|^2}\right) \\ &-\frac{(|\mathbf{r}-\mathbf{r}_{\mathrm{i}}| + |\mathbf{r}-\mathbf{r}_{\mathrm{i+1}}|)^2(|\mathbf{r}-\mathbf{r}_{\mathrm{i+1}}|(y-y_{\mathrm{i}}) + |\mathbf{r}-\mathbf{r}_{\mathrm{i}}|(y-y_{\mathrm{i+1}}))}{|\mathbf{r}-\mathbf{r}_{\mathrm{i}}|^2|\mathbf{r}-\mathbf{r}_{\mathrm{i+1}}|^2(|\mathbf{r}-\mathbf{r}_{\mathrm{i}}||\mathbf{r}-\mathbf{r}_{\mathrm{i+1}}| + (\mathbf{r}-\mathbf{r}_{\mathrm{i}})(\mathbf{r}-\mathbf{r}_{\mathrm{i+1}}))^2}\end{aligned} \tag{18}$$

$$\begin{aligned}\frac{\partial f(\mathbf{r})}{\partial z} = &\frac{-1}{(|\mathbf{r}-\mathbf{r}_{\mathrm{i}}||\mathbf{r}-\mathbf{r}_{\mathrm{i+1}}| + (\mathbf{r}-\mathbf{r}_{\mathrm{i}})(\mathbf{r}-\mathbf{r}_{\mathrm{i+1}}))|\mathbf{r}-\mathbf{r}_{\mathrm{i}}||\mathbf{r}-\mathbf{r}_{\mathrm{i+1}}|} \\ &\cdot\left(\frac{(z-z_{\mathrm{i}})|\mathbf{r}-\mathbf{r}_{\mathrm{i+1}}|}{|\mathbf{r}-\mathbf{r}_{\mathrm{i}}|^2} + \frac{(z-z_{\mathrm{i+1}})|\mathbf{r}-\mathbf{r}_{\mathrm{i}}|}{|\mathbf{r}-\mathbf{r}_{\mathrm{i+1}}|^2}\right)\end{aligned} \tag{19}$$

$$-\frac{(|\mathbf{r}-\mathbf{r}_{\mathrm{i}}|+|\mathbf{r}-\mathbf{r}_{\mathrm{i+1}}|)^2(|\mathbf{r}-\mathbf{r}_{\mathrm{i+1}}|(z-z_{\mathrm{i}})+|\mathbf{r}-\mathbf{r}_{\mathrm{i}}|(z-z_{\mathrm{i+1}}))}{|\mathbf{r}-\mathbf{r}_{\mathrm{i}}|^2|\mathbf{r}-\mathbf{r}_{\mathrm{i+1}}|^2(|\mathbf{r}-\mathbf{r}_{\mathrm{i}}||\mathbf{r}-\mathbf{r}_{\mathrm{i+1}}|+(\mathbf{r}-\mathbf{r}_{\mathrm{i}})(\mathbf{r}-\mathbf{r}_{\mathrm{i+1}}))^2}$$

the first derivatives of the magnetic field, $\mathbf{B}^{\mathrm{i}}$, are given by

$$\frac{\partial \mathbf{B}^{\mathrm{i}}_x}{\partial x}=\frac{\mu_0}{4\pi}I_{\mathrm{i}}((y-y_{\mathrm{i}})(z-z_{\mathrm{i+1}})-(z-z_{\mathrm{i}})(y-y_{\mathrm{i+1}}))\frac{\partial f(\mathbf{r})}{\partial x}$$

$$\frac{\partial \mathbf{B}^{\mathrm{i}}_x}{\partial y}=\frac{\mu_0}{4\pi}I_{\mathrm{i}}\left[((z-z_{\mathrm{i+1}})-(z-z_{\mathrm{i}}))f(\mathrm{r})+((y-y_{\mathrm{i}})(z-z_{\mathrm{i+1}})-(z-z_{\mathrm{i}})(y-y_{\mathrm{i+1}}))\frac{\partial f(\mathbf{r})}{\partial y}\right] \quad (20)$$

$$\frac{\partial \mathbf{B}^{\mathrm{i}}_x}{\partial z}=\frac{\mu_0}{4\pi}I_{\mathrm{i}}\left[((y-y_{\mathrm{i}})-(y-y_{\mathrm{i+1}}))f(\mathrm{r})+((y-y_{\mathrm{i}})(z-z_{\mathrm{i+1}})-(z-z_{\mathrm{i}})(y-y_{\mathrm{i+1}}))\frac{\partial f(\mathbf{r})}{\partial z}\right]$$

$$\frac{\partial \mathbf{B}^{\mathrm{i}}_y}{\partial x}=\frac{\mu_0}{4\pi}I_{\mathrm{i}}\left[((z-z_{\mathrm{i}})-(z-z_{\mathrm{i+1}}))f(\mathrm{r})+((z-z_{\mathrm{i}})(x-x_{\mathrm{i+1}})-(x-x_{\mathrm{i}})(z-z_{\mathrm{i+1}}))\frac{\partial f(\mathbf{r})}{\partial x}\right]$$

$$\frac{\partial \mathbf{B}^{\mathrm{i}}_y}{\partial y}=\frac{\mu_0}{4\pi}I_{\mathrm{i}}((z-z_{\mathrm{i}})(x-x_{\mathrm{i+1}})-(x-x_{\mathrm{i}})(z-z_{\mathrm{i+1}}))\frac{\partial f(\mathbf{r})}{\partial y} \quad (21)$$

$$\frac{\partial \mathbf{B}^{\mathrm{i}}_y}{\partial z}=\frac{\mu_0}{4\pi}I_{\mathrm{i}}\left[((x-x_{\mathrm{i+1}})-(x-x_{\mathrm{i}}))f(\mathrm{r})+((z-z_{\mathrm{i}})(x-x_{\mathrm{i+1}})-(x-x_{\mathrm{i}})(z-z_{\mathrm{i+1}}))\frac{\partial f(\mathbf{r})}{\partial z}\right]$$

$$\frac{\partial \mathbf{B}^{\mathrm{i}}_z}{\partial x}=\frac{\mu_0}{4\pi}I_{\mathrm{i}}\left[((y-y_{\mathrm{i+1}})-(y-y_{\mathrm{i}}))f(\mathrm{r})+((x-x_{\mathrm{i}})(y-y_{\mathrm{i+1}})-(y-y_{\mathrm{i}})(x-x_{\mathrm{i+1}}))\frac{\partial f(\mathbf{r})}{\partial x}\right]$$

$$\frac{\partial \mathbf{B}^{\mathrm{i}}_z}{\partial y}=\frac{\mu_0}{4\pi}I_{\mathrm{i}}\left[((x-x_{\mathrm{i}})-(x-x_{\mathrm{i+1}}))f(\mathrm{r})+((x-x_{\mathrm{i}})(y-y_{\mathrm{i+1}})-(y-y_{\mathrm{i}})(x-x_{\mathrm{i+1}}))\frac{\partial f(\mathbf{r})}{\partial y}\right] \quad (22)$$

$$\frac{\partial \mathbf{B}^{\mathrm{i}}_z}{\partial z}=\frac{\mu_0}{4\pi}I_{\mathrm{i}}((x-x_{\mathrm{i}})(y-y_{\mathrm{i+1}})-(y-y_{\mathrm{i}})(x-x_{\mathrm{i+1}}))\frac{\partial f(\mathbf{r})}{\partial z}$$

B.2 TRANSFORMATION INTO CYLINDRICAL CO-ORDINATES

- Magnetic field

$$B_R = B_x \cos\varphi + B_y \sin\varphi, \quad B_\varphi = B_y \cos\varphi - B_x \sin\varphi, \quad B_Z = B_z \tag{23}$$

- First derivatives of the magnetic field

$$\frac{\partial B_R}{\partial R} = \frac{\partial B_x}{\partial x}\cos^2\varphi + \frac{\partial B_y}{\partial y}\sin^2\varphi + \left(\frac{\partial B_x}{\partial y} + \frac{\partial B_y}{\partial x}\right)\sin\varphi\cos\varphi$$

$$\frac{\partial B_R}{\partial \varphi} = \frac{\partial B_x}{\partial y}R\cos^2\varphi - \frac{\partial B_y}{\partial x}R\sin^2\varphi + \left(\frac{\partial B_y}{\partial y} - \frac{\partial B_x}{\partial x}\right)R\sin\varphi\cos\varphi - B_x\sin\varphi + B_y\cos\varphi \tag{24}$$

$$\frac{\partial B_R}{\partial Z} = \frac{\partial B_x}{\partial z}\cos\varphi + \frac{\partial B_y}{\partial z}\sin\varphi$$

$$\frac{\partial B_\varphi}{\partial R} = \frac{\partial B_y}{\partial x}\cos^2\varphi - \frac{\partial B_x}{\partial y}\sin^2\varphi + \left(\frac{\partial B_y}{\partial y} - \frac{\partial B_x}{\partial x}\right)\sin\varphi\cos\varphi$$

$$\frac{\partial B_\varphi}{\partial \varphi} = \frac{\partial B_y}{\partial y}R\cos^2\varphi + \frac{\partial B_x}{\partial x}R\sin^2\varphi - \left(\frac{\partial B_y}{\partial x} + \frac{\partial B_x}{\partial y}\right)R\sin\varphi\cos\varphi - B_y\sin\varphi - B_x\cos\varphi \tag{25}$$

$$\frac{\partial B_\varphi}{\partial Z} = \frac{\partial B_y}{\partial z}\cos\varphi - \frac{\partial B_x}{\partial z}\sin\varphi$$

$$\frac{\partial B_Z}{\partial R} = \frac{\partial B_z}{\partial x}\cos\varphi + \frac{\partial B_z}{\partial y}\sin\varphi$$

$$\frac{\partial B_Z}{\partial \varphi} = \frac{\partial B_z}{\partial y}R\cos\varphi - \frac{\partial B_z}{\partial x}R\sin\varphi \tag{26}$$

$$\frac{\partial B_Z}{\partial Z} = \frac{\partial B_z}{\partial z}$$

B.3 STELLARATOR SYMMETRY

In cylindrical co-ordinates the magnetic field at point $\mathbf{r} = (R, \varphi, Z)$ is related to the field at the stellarator symmetric point $\mathbf{r}' = (R, 2\pi/N_\mathrm{p} - \varphi, -Z)$:

- Magnetic field strength

$$B(\mathbf{r}') = B(\mathbf{r}) \tag{27}$$

- Magnetic field components

$$B_R(\mathbf{r}') = -B_R(\mathbf{r}), \quad B_\varphi(\mathbf{r}') = B_\varphi(\mathbf{r}), \quad B_Z(\mathbf{r}') = B_Z(\mathbf{r}) \tag{28}$$

- First derivatives

$$\frac{\partial B_R}{\partial R}(\mathbf{r}') = -\frac{\partial B_R}{\partial R}(\mathbf{r}), \quad \frac{\partial B_R}{\partial \varphi}(\mathbf{r}') = \frac{\partial B_R}{\partial \varphi}(\mathbf{r}), \quad \frac{\partial B_R}{\partial Z}(\mathbf{r}') = \frac{\partial B_R}{\partial Z}(\mathbf{r})$$

$$\frac{\partial B_\varphi}{\partial R}(\mathbf{r}') = \frac{\partial B_\varphi}{\partial R}(\mathbf{r}), \quad \frac{\partial B_\varphi}{\partial \varphi}(\mathbf{r}') = -\frac{\partial B_\varphi}{\partial \varphi}(\mathbf{r}), \quad \frac{\partial B_\varphi}{\partial Z}(\mathbf{r}') = -\frac{\partial B_\varphi}{\partial Z}(\mathbf{r}) \tag{29}$$

$$\frac{\partial B_Z}{\partial R}(\mathbf{r}') = \frac{\partial B_Z}{\partial R}(\mathbf{r}), \quad \frac{\partial B_Z}{\partial \varphi}(\mathbf{r}') = -\frac{\partial B_Z}{\partial \varphi}(\mathbf{r}), \quad \frac{\partial B_Z}{\partial Z}(\mathbf{r}') = -\frac{\partial B_Z}{\partial Z}(\mathbf{r})$$